RSC Advances

PAPER

View Article Online
View Journal | View Issue

Cite this: *RSC Adv.*, 2019, **9**, 7078

Preparation and spectral characteristics of Tm^{3+}/Ho^{3+} co-doped TeO_2–B_2O_3–BaO glass

Qingbo Wang, Junying Zhang, Weimin Dong, Lintao Liu, Hang Wen, Qian Yao, Jing Li* and Jiyang Wang

Received 4th December 2018
Accepted 16th February 2019

DOI: 10.1039/c8ra09971e

rsc.li/rsc-advances

TeO–B_2O_3–BaO glasses with different compositions were prepared by the conventional melt-quenching technique. The spectral properties of Tm^{3+}/Ho^{3+} co-doped TeO–B_2O_3–BaO glasses with different doping concentrations were studied. In order to analyze the spectroscopic properties in detail, the Judd–Ofelt intensity parameters, spontaneous radiative probabilities, branching ratios, absorption and emission cross-sections, and gain coefficient spectra were calculated using Judd–Ofelt and McCumber theory based on the absorption and emission spectra. Meanwhile, the optimal doping concentration was determined as Tm_2O_3: 1.0 mol% and Ho_2O_3: 1.0 mol%. The results show that Tm^{3+}/Ho^{3+} co-doped TeO–B_2O_3–BaO glass is an ideal mid-infrared laser gain medium.

Introduction

In recent years, infrared lasers working around 2 μm have attracted widespread attention because of their wide range of uses, such as in eye-safe lidar systems, laser remote sensing, biomedical uses.[1,2] It is well-known that lasers at around 2 μm can be obtained from the Ho^{3+}:$^5I_7 \rightarrow {}^5I_8$ or Tm^{3+}:$^3F_4 \rightarrow {}^3H_6$ transition processes. Ho^{3+} ions have a wide radiation bandwidth and long fluorescence lifetime, and the stimulated emission cross-section is larger than that of Tm^{3+} ions.[3–5] However, due to the lack of a corresponding absorption band, Ho^{3+}-doped lasers cannot be directly pumped by commercially available 808 nm or 980 nm LD pump sources. Other rare-earth ions such as Yb^{3+}, Er^{3+}, and Tm^{3+} have an absorption band at 808 nm or 980 nm and can be introduced as a sensitizer co-doped with Ho^{3+}. Among them, Tm^{3+} has a strong absorption band at 808 nm and can be directly pumped by an 808 nm LD, which has attracted widespread interest.[6–8] In order to obtain a strong laser output at around 2 μm, a series of laser glasses have been developed. Compared with other matrix materials such as silicate glass, germanate glass, and halide and sulfide glass, tellurate glass has good thermal stability, low thermal expansion coefficient and good solubility of rare-earth ions.[9] It is generally believed that tellurium ions in tellurate glass are mainly in the form of trigonal bipyramid [TeO_4], deformed trigonal bipyramid [TeO_{3+1}] and trigonal pyramid [TeO_3]. These structural groups are linked to each other at a certain angle to form a long chain or a ring chain.[10] BaO exists in glass as a network modifier and does not participate in network construction. With the addition of BaO, the trigonal bipyramid [TeO_4] transforms into the deformed trigonal bipyramid [TeO_{3+1}] and trigonal pyramid [TeO_3].[11,12] Furthermore, more BaO enters the gap between these long chains or ring chains in the form of [BaO_6] and [BaO_7] polyhedra, making the network of glass more compact, which improves the mechanical strength and thermal stability of the glass.[13] The introduction of B_2O_3 improves the thermal stability and contributes to the formation of glass.

Here, Tm^{3+}/Ho^{3+} co-doped tellurate glasses with different compositions of TeO_2–B_2O_3–BaO were prepared, and an emission peak at around 2.0 μm was obtained under the excitation of an 808 nm LD. We investigate the appropriate co-doping concentrations of Tm^{3+} and Ho^{3+} that can output an intense ultra-broad fluorescence emission band at around 2.0 μm. Meanwhile, the energy transfer mechanism between Tm^{3+} and Ho^{3+} was systematically analyzed. In addition, quantitative research was conducted based on Judd–Ofelt theory in order to evaluate the radiation performance of Tm^{3+} and Ho^{3+}. After that, the absorption and emission cross-sections and gain coefficient spectra were calculated and discussed on the basis of the absorption and emission spectra.

Experimental

Material synthesis

Undoped TeO_2–B_2O_3–BaO glasses with different compositions and Tm^{3+}/Ho^{3+} co-doped TeO_2–B_2O_3–BaO glasses with different doping concentrations were prepared by the traditional melt-quenching method. 10 g of powders of TeO_2, $BaCO_3$, H_3BO_3, Tm_2O_3 and Ho_2O_3 were weighed exactly according to the ratio, mixed well and poured into a platinum crucible, and kept at 450 °C for one hour to remove gas and moisture. Then, the temperature was raised to 850 °C, and the mixture was melted

State Key Lab of Crystal Materials, Shandong University, Jinan 250100, China. E-mail: jingli@sdu.edu.cn

for 30 minutes and stirred. The purpose of the stirring is to uniformly mix the raw materials and remove the bubbles in the glass to homogenize the molten glass. The molten glass was poured onto a preheated stencil and quickly transferred to a preheated resistance furnace (the furnace temperature is near the transition temperature of the glass sample) to anneal the sample and eliminate stress in the glass. The temperature was kept near the glass transition temperature for 4 hours and then the sample was naturally cooled to room temperature. The annealed glass samples were processed into a certain size and shape according to the relevant test requirements, and were polished for related tests such as infrared transmission, absorption and fluorescence spectroscopy.

Measurements

Thermal performance analysis of powder samples crushed down from the samples was achieved by a Diamond TG/DTA from Perkin Elmer, USA. The test temperature range was 200–550 °C, the heating rate was 10 °C min^{-1}, and the analysis was performed in an air atmosphere. The Raman and infrared transmission spectra of the glass samples were measured by a NEXUS 670 Fourier transform infrared-Raman (FT-IR & Raman) spectrometer from Thermo Nicolet, USA. The test ranges were 250–1800 cm^{-1} and 400–4000 cm^{-1}, respectively. The transmission spectrum of the undoped TeO_2–B_2O_3–BaO glass samples and the absorption spectrum of the Tm^{3+}/Ho^{3+} co-doped TeO_2–B_2O_3–BaO glass samples were, respectively, measured using a U-3500 IR/VIS/UV spectrophotometer manufactured by Hitachi. Fluorescence spectra and lifetimes were measured using an FLSP 980 time-resolved steady-state/transient spectrometer from Edinburgh Instruments. The excitation sources were 980 nm and 808 nm LDs, respectively. All of the measurements were carried out at room temperature.

Results and discussion

Glass samples

In this work, TeO_2–B_2O_3–BaO glass substrates with glass compositions as follows: 33%TeO_2–34%B_2O_3–33%BaO (TBB1), 60%TeO_2–20%B_2O_3–20%BaO (TBB2), 67%TeO_2–17%B_2O_3–16%BaO (TBB3), 70%TeO_2–10%B_2O_3–20%BaO (TBB4) and 50%TeO_2–30%B_2O_3–20%BaO (TBB5), were prepared. Glass samples with the compositions $1Tm_2O_3$–xHo_2O_3–$(99 - x)$(TeO_2–B_2O_3–BaO) (x = 0, 0.6, 1.0, 1.5, 2.0, 3.0 mol%) and xTm_2O_3–$1Ho_2O_3$–$(99 - x)$(TeO_2–B_2O_3–BaO) (x = 0, 0.2, 0.5, 1.0, 1.5 mol%) were also prepared, and de-noted as TBBTH0, TBBTH0.6, TBBTH1.0, TBBTH1.5, TBBTH2.0, TBBTH3.0, and TBBHT0, TBBHT0.2, TBBHT0.5, and TBBTH1.0, TBBHT1.5, respectively. Pictures of these samples are shown in Fig. 1.

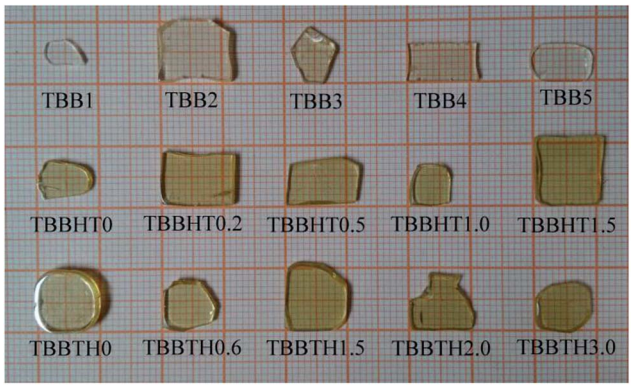

Fig. 1 TeO_2–B_2O_3–BaO glass substrates with different glass compositions and glass samples with different doping concentrations.

Raman spectra

Raman spectroscopy can reflect the condition of the internal structure of the glass, which has an important influence on its thermal properties, spectral properties, *etc.* Fig. 2 presents the Raman spectra of the glass samples with a test range of 250–1800 cm^{-1}. In these Raman spectra, the spectral band appearing at 160–190 cm^{-1} corresponds to the vibration of Ba^{2+}. The peak at 450–475 cm^{-1} corresponds to the Te–O–Te or O–Te–O bending vibration. The peak at 550–560 cm^{-1} corresponds to the vibration of [BO^{4-}], and the peak at 670–680 cm^{-1} corresponds to the asymmetric stretching vibration of the Te–O bond in [TeO_4]. The Raman band at 750–770 cm^{-1} corresponds to the symmetric stretching vibration of Te–O in [TeO_3] and [TeO^{3+1}].[14,15]

The peak with the largest wave number in the Raman spectrum represents the phonon energy of the matrix. The higher the phonon energy of the glass matrix, the greater the multi-phonon relaxation rate, which affects the radiation transition in the mid-infrared region, making fluorescence quenching more likely to occur in the glass. As can be seen from Fig. 2, the phonon energies of the glass substrates are 772 cm^{-1}, 762 cm^{-1}, 689 cm^{-1}, 692 cm^{-1} and 756 cm^{-1}, respectively, and are smaller than those of other glass substrates such as silicate (~1100 cm^{-1}), germanate (~900 cm^{-1}), *etc.* This indicates that the TeO_2–B_2O_3–BaO glass system has the conditions required for use as a mid-infrared laser gain medium.

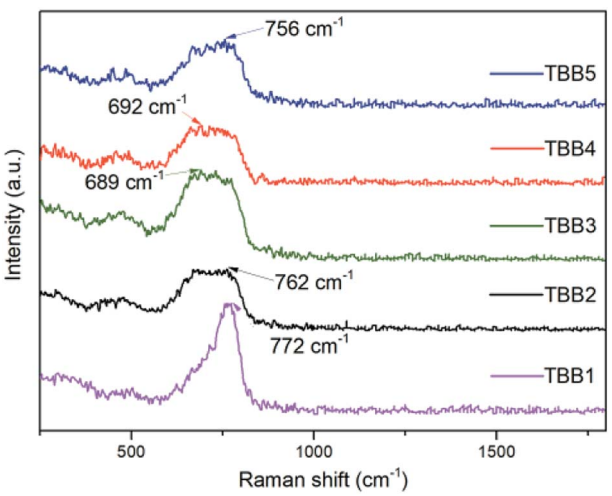

Fig. 2 Raman spectra of the glass substrates.

OH^- group content

The strong vibration of each group in the glass network has a great influence on the intrinsic absorption.[16] In the matrix material, an increase in the OH^- content weakens the glass network structure, which in turn affects its absorption of infrared light. For mid-infrared laser glass materials, OH^- can greatly reduce the fluorescence intensity and affect the fluorescence output in the mid-infrared band through the multi-phonon quenching mechanism. The infrared transmission spectrum of each glass sample is shown in Fig. 3. From the spectrum and the following formula:

$$\alpha = \frac{\ln(I_0/I)}{l}$$

where I_0 is the maximum transmittance of the glass, I is the transmittance near 3000 nm and l is the thickness of the glass sample, the absorption coefficient (α) of the hydroxyl groups in the sample can be determined. The calculated hydroxyl absorption coefficients in each sample are listed in Table 1. It is deduced that the hydroxyl content of TBB3 is relatively small.

Thermal stability

Thermal stability is one of the important parameters for measuring the properties of glass. Generally, ΔT ($=T_x - T_g$) is used to characterize the thermal stability of a glass. A large value of ΔT means that inhibition of crystallization and nucleation is strong, and the thermal stability is good. As can be seen in Fig. 4, the glass transition temperature (T_g) and crystallization temperature (T_x) increase with increasing B_2O_3 content. TBB1 and TBB5 did not observe significant crystallization peaks within the test range. The transition temperature of TBB3 is 375 °C and the crystallization temperature is 481 °C. Among the TBB2, TBB3 and TBB4 glass samples, only the ΔT of the TBB3 glass sample was larger than 100 °C ($\Delta T = 106$ °C), indicating that the TBB3 glass has good thermal stability.

Table 1 The hydroxyl absorption coefficient of each glass

Glass	TBB1	TBB2	TBB3	TBB4	TBB5
α (cm^{-1})	4.769	7.324	4.49	5.59	5.77

A comprehensive comparison of the properties of the prepared undoped glass samples was carried out, and the TBB3 glass with less phonon energy, lower relative hydroxyl content and better thermal stability was selected as the matrix material for subsequent Tm^{3+}/Ho^{3+} doping.

Absorption spectrum and Judd–Ofelt analysis

Fig. 5 displays the measured absorption spectra of Tm^{3+} and Ho^{3+} single-doped and Tm^{3+}/Ho^{3+} co-doped TeO_2–B_2O_3–BaO glass at 300–2500 nm. For the Ho^{3+} single-doped sample, the absorption spectrum was found to contain absorption bands centered at wavelengths of 420 nm, 452 nm, 486 nm, 538 nm, 644 nm, 902 nm, 1158 nm, and 1946 nm, which in turn correspond to the transitions from the ground state $^5I_8$ to the excited states $^5G_5$, $^5G_6 + {}^5F_1$, $^5F_3$, $^5S_2 + {}^5F_4$, $^5F_5$, $^5I_5$, $^5I_6$, and $^5I_7$. For the Tm^{3+} single-doped sample, the absorption spectrum has five absorption bands at 466 nm, 686 nm, 792 nm, 1208 nm, and 1695 nm, which are attributed to the transition from the ground state $^3H_6$ to the excited states $^1G_4$, $^3F_3$, $^3H_4$, $^3H_5$ and $^3F_4$, respectively. In the Ho^{3+}/Tm^{3+} co-doped sample, the absorption spectrum shows a superposition of Ho^{3+} and Tm^{3+} ion absorption peaks, and the positions of the respective absorption peaks did not change substantially.

The measured absorption spectrum can be analyzed by J–O theory for the radiation transition characteristics in the $4f^N$ structure of rare-earth ions.[17,18] Based on J–O theory, the experimental oscillator strength (f_{exp}) can be obtained using the following formula:

$$f_{exp} = \frac{mc^2}{0.43d\bar{\lambda}^2e^2N\pi}\int \mathrm{OD}(\lambda)\mathrm{d}\lambda$$

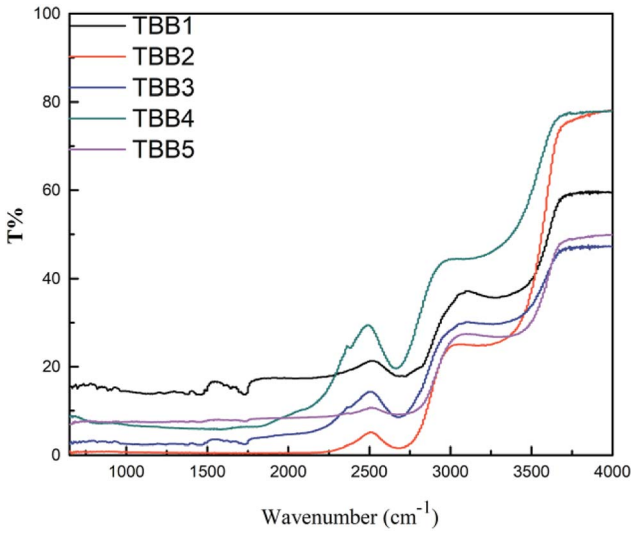

Fig. 3 Infrared transmission spectra of the glass samples.

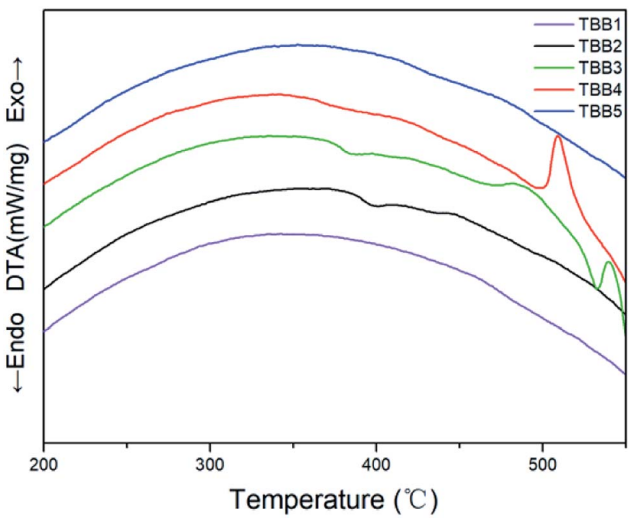

Fig. 4 The DTA curves of the un-doped glass samples.

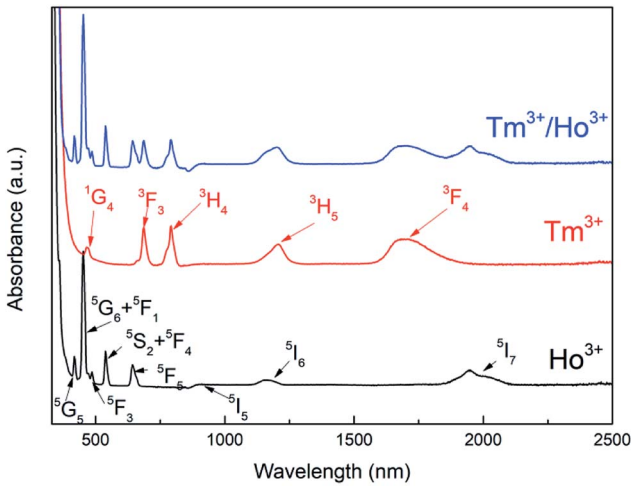

Fig. 5 Absorption spectra of Tm^{3+} and Ho^{3+} single doped and Tm^{3+}/Ho^{3+} co-doped glasses.

where m is the electronic mass (9.109×10^{-31} kg), e is the electron charge (6.02×10^{-19} C), c is the speed of light in a vacuum (2.998×10^{-8} m s^{-1}), d is the sample thickness, N is the rare earth ion concentration, $\bar{\lambda}$ is the mean wavelength and OD (λ) is the optical density.

The theoretical oscillator strength can be obtained using the following equation:

$$f_{cal} = f_{ed} + f_{md}$$

where f_{ed} and f_{md} are the electric dipole and magnetic dipole transition oscillator strengths, respectively, and their respective expressions are as follows:

$$f_{ed} = \frac{8\pi^2 mc}{3h(2J+1)\bar{\lambda}}\chi_{ed}S^{ed}$$

$$f_{md} = \frac{8\pi^2 mc}{3h(2J+1)\bar{\lambda}}\chi_{md}S^{md}$$

where h is Planck's constant, J is the total angular momentum quantum number, χ_{ed} and χ_{md} are the correction factors for the electric- and magnetic-dipole absorption transitions, and S_{ed} and S_{md} are the electric- and magnetic-dipole transition line intensities of the transition from the $S\,L\,J$ level to $S'\,L'\,J'$ level, respectively.

The Judd–Ofelt parameters and related spectral performance parameters of the Ho^{3+} ions in the TBBTH1.0 samples were calculated. Table 2 shows the experimental and theoretical oscillator strength of the Ho^{3+} in the glass sample. The root mean square error $\delta = 0.81 \times 10^{-6}$, indicating that the calculation results are credible. The corresponding Judd–Ofelt intensity parameter Ω_t was obtained by fitting. Table 3 shows the Ω_t values of Ho^{3+} ions in TBB3 and other usual glass matrixes. Ω_2 is closely related to the symmetry and order of the coordination field. The smaller the Ω_2, the weaker the covalency of the bond between the rare-earth atom and the oxygen atom. It

Table 2 f_{exp} and f_{cal} of Ho^{3+} ions in co-doped glass[a]

Final state	λ	f_{exp} ($\times 10^{-6}$)	f_{cal} ($\times 10^{-6}$)
$^5G_5$	418	3.99	3.91
$^5F_1 + {}^5G_6$	452	30.9	30.4
$^5F_4 + {}^5S_2$	538	6.19	5.12
$^5F_5$	644	3.75	3.93
$^5I_6$	1154	1.06	1.45

[a] $\Omega_2 = 5.62 \times 10^{-20}$, $\Omega_4 = 2.46 \times 10^{-20}$, $\Omega_6 = 1.72 \times 10^{-20}$, $\delta = 0.81 \times 10^{-6}$.

Table 3 Comparison of the Ω_t values in different glasses with Ho^{3+} doping

Glass host	Ω_2	Ω_4	Ω_6
Fluoride[19]	1.86	1.90	1.32
Phosphate[20]	3.33	3.01	0.61
Silicate[21]	3.14	3.04	4.97
Sulfide[22]	0.1	4.97	0.98
Germanate[23]	7.83	6.37	2.05
TBBTH1.0[this work]	5.62	2.46	1.72

can be seen from the table that the Ω_2 value of TeO_2–B_2O_3–BaO glass is larger than that of other glass substrates such as fluoride, silicate and phosphate glass. This may be due to the presence of multiple polyhedral structural units in the glass. The value of Ω_6 is related to the spontaneous radiation probability (A_{rad}), which becomes larger as the value of Ω_6 increases, and the large A_{rad} is favorable for obtaining luminescence in the 2 μm band. In the TeO_2–B_2O_3–BaO glass system, the value of Ω_6 is larger than that in fluoride glass, phosphate glass and sulfide glass, and slightly smaller than that in germanate glass, indicating that the TeO_2–B_2O_3–BaO glass system has better radiation transition properties.

According to the Ω_t value calculated in Table 3, the main spectral parameters of the Ho^{3+} transitions at different energy levels in glass sample were further calculated, such as the spontaneous radiation probability (A_{rad}), the branching ratio (β) and the radiation lifetime (τ), using the following formulae:

$$A_{rad} = \frac{64\pi^4 e^2}{3h(2J+1)\bar{\lambda}^3}\left[\frac{n(n^2+2)^2}{9}S^{ed} + n^3 S^{md}\right]$$

$$\tau_{rad} = \frac{1}{\sum_{\gamma' J'} A_{rad}\left[\gamma J, \gamma' J'\right]}$$

$$\beta = \frac{A_{rad}\left[\gamma J, \gamma' J'\right]}{\sum_{\gamma' J'} A_{rad}\left[\gamma J, \gamma' J'\right]}$$

where h, e, J, $\bar{\lambda}$, S_{ed} and S_{md} have the same meanings as above. n is the sample refractive index. The calculation results are shown in Table 4. It can be seen from Table 4 that the spontaneous

Table 4 A_{rad}, β and τ of Ho^{3+} ions in glass samples

	A_{ed}	A_{md}	A_{rad}/s^{-1}	β/%	τ/ms
$^5I_7 \rightarrow {}^5I_8$	142.11	43.74	185.85	100	5.38
$^5I_6 \rightarrow {}^5I_7$	26.14	28.76	280.33	80.4	3.57
$^5I_8$	225.43				
$^5I_5 \rightarrow {}^5I_6$	9.715	13.066	207.301	38.1	4.82
$^5I_7$	105.48				
$^5I_8$	79.04				
$^5F_5 \rightarrow {}^5I_5$	10.49		3366.57	76.7	0.30
$^5I_6$	134.08				
$^5I_7$	641.30				
$^5I_8$	2580.70				
$^5F_4 \rightarrow {}^5F_5$	15.96	8.215	5834.97	79.2	0.17
$^5I_5$	191.59				
$^5I_6$	392.80				
$^5I_7$	603.56				
$^5I_8$	4622.84				

radiation probability of Ho^{3+}:$^4I_7 \rightarrow {}^5I_8$ in the glass sample that produces a 2 μm fluorescence band is 185.85 s^{-1}, which is higher than that in other matrix materials such as germanate glass (94.5 s^{-1}), fluoride glass (73.04 s^{-1}) and silicate glass (71.64 s^{-1}).[24–26] The larger the value of A_{rad}, the greater the probability of laser generation, and the more favorable it is for the output of the 2 μm laser.[27]

Fluorescence spectroscopy and concentration optimization

Fig. 6 shows the fluorescence spectrum in the mid-infrared range of Tm^{3+}/Ho^{3+} co-doped glass with different Ho^{3+} doping concentrations under 808 nm excitation. The inset is a plot of the change in fluorescence intensity and fluorescence lifetime in glass samples with different Ho_2O_3 concentrations. There are mainly two luminescence peaks in Fig. 6, wherein the fluorescence peak of the Tm^{3+} single-doped sample is located near 1.8 μm, corresponding to the radiation transition of Tm^{3+}:$^3F_4 \rightarrow {}^3H_6$. In the Tm^{3+}/Ho^{3+} co-doped sample, the fluorescence peak appeared at around 2.0 μm, corresponding to the Ho^{3+}:$^5I_7 \rightarrow {}^5I_8$ radiation transition. As the concentration of Ho^{3+} ions increases, the 1.8 μm luminescence peak gradually decreases, and due to the fluorescence quenching phenomenon caused by the high concentration of Ho^{3+}, the fluorescence intensity at around 2 μm increases first and then decreases. Though the fluorescence lifetime suddenly decreases from TBBTH1.5 glass, there is no great difference between TBBTH0.6 and TBBTH1.0 and the intensity of the luminescence peak near 2.0 μm is the largest when the doping concentration of Ho_2O_3 is 1 mol%. It can be seen from the absorption spectrum in Fig. 5 that Ho^{3+} has no absorption peak near 808 nm, which indicates that there is an energy transfer process between Tm^{3+} and Ho^{3+}. The energy level diagrams and energy transfer processes of Tm^{3+} and Ho^{3+} are shown in Fig. 7. Tm^{3+} ions first transition from the $^3H_6$ level to the $^3H_4$ level under excitation of 808 nm, and then they transfer to the $^3F_4$ level manifold quickly in three ways. The first approach is that the Tm^{3+} ions in the excited state radiatively transfer to the $^3F_4$ level and emit photons at 1.47 μm, the second is the cross-relaxation process between the Tm^{3+}:$^3H_4$ state and Tm^{3+}:$^3H_6$ state ($^3H_4 + {}^3H_6 \rightarrow {}^3F_4 + {}^3F_4$), and the last one is ET1 in Fig. 7, which is indicated as: $^3H_4$(Tm) + $^5I_8$(Ho) → $^3F_4$(Tm) + $^5I_7$(Ho), but it is so weak that we usually ignore it. Because the Tm^{3+}:$^3F_4$ state and the Ho^{3+}:$^5I_7$ state are very close, Tm^{3+} ions in the $^3F_4$ state transfer their energy to the Ho^{3+}:$^5I_7$ in the metastable state *via* $^3F_4 + {}^5I_8 \rightarrow {}^3H_6 + {}^5I_7$ (ET2). Finally, Ho^{3+} produces fluorescence at around 2.0 μm by the transition from $^5I_7$ to $^5I_8$.

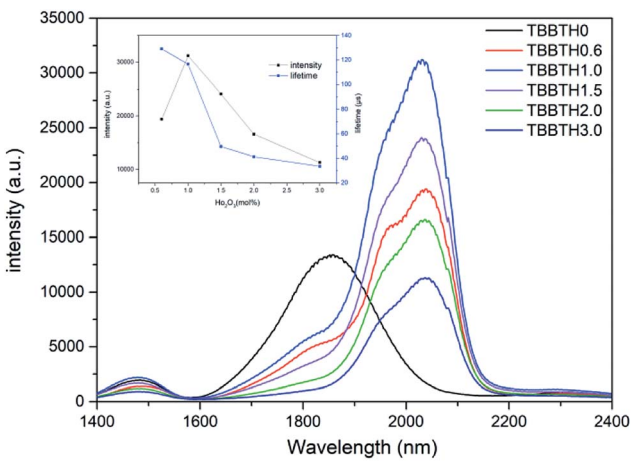

Fig. 6 Fluorescence spectra of Tm^{3+}/Ho^{3+} co-doped TeO_2–B_2O_3–BaO glass with different concentrations of Ho^{3+}. The inset is a plot of the change of fluorescence intensity and fluorescence lifetime in glass samples with different Ho_2O_3 concentrations.

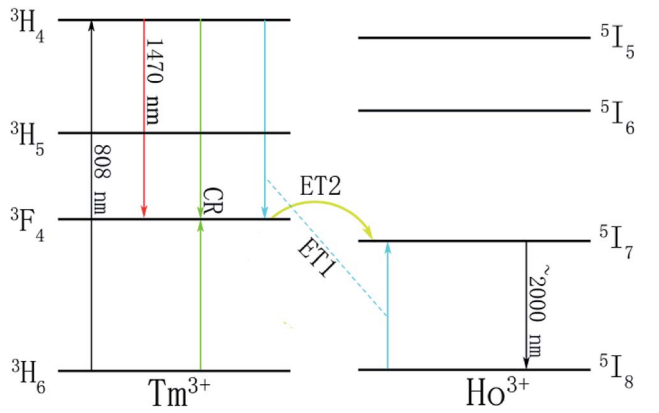

Fig. 7 Energy level scheme of Tm^{3+} and Ho^{3+} ions.

In addition, in order to further analyze the influence of different concentrations of Tm^{3+} ions on the optical properties of the glass and to explore the optimal doping concentration, the doping concentration of Ho_2O_3 was fixed at 1 mol%, and the doping concentration of Tm_2O_3 was set as 0, 0.2, 0.5, 1.0 and 1.5 mol%, respectively. Fig. 8 is the fluorescence spectra of the Tm^{3+}/Ho^{3+} co-doped glass samples with different concentrations of Tm^{3+} excited by an 808 nm laser. The inset shows the trend in fluorescence intensity of the glass samples with different Tm_2O_3 concentrations. When the concentration of Tm^{3+} increases from 0.2 mol% to 1 mol%, the fluorescence

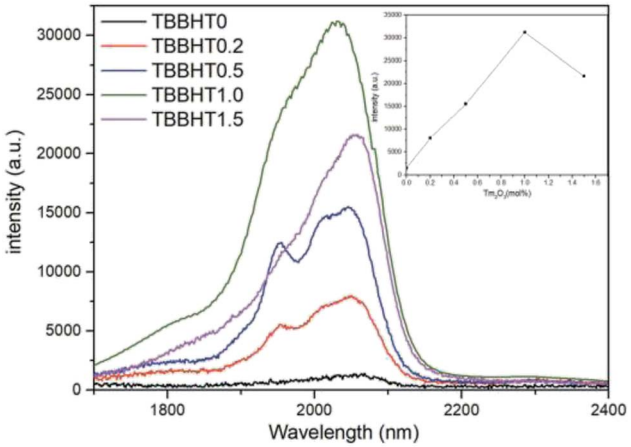

Fig. 8 Fluorescence spectra of Tm^{3+}/Ho^{3+} co-doped TeO_2–B_2O_3–BaO glass with different concentrations of Tm^{3+}. The inset is the trend of fluorescence intensity of glass samples with different Tm_2O_3 concentrations.

intensity near 2.0 μm gradually increases, and when the concentration continues to increase, the fluorescence intensity decreases. Therefore, it can be considered that a suitable concentration of Tm^{3+}/Ho^{3+} co-doping in the glass system is Tm_2O_3: 1.0 mol% and Ho_2O_3: 1.0 mol%.

Emission cross-section and gain characteristics

The sample with a doping concentration of Tm_2O_3: 1.0 mol% and Ho_2O_3: 1.0 mol%, which is the optimum doping concentration, was selected to calculate the absorption and emission cross-sections from its absorption spectrum using the McCumber theory. The absorption cross-section (σ_{abs}) of the ground state energy level to the excited state energy level can be calculated from the absorption spectrum using the following formula:

$$\sigma_{abs}(\lambda) = \frac{1}{Nl}\log\frac{I_0}{I} = \frac{2.303}{Nl}\mathrm{OD}(\lambda)$$

where N, l, I_0, I and OD(λ), respectively, represent the doping concentration of rare-earth ions, the sample thickness, the input and transmit intensity, and the optical density.

The stimulated emission cross-section is an important parameter for evaluating the performance of laser glass. The stimulated emission cross-section of rare-earth ions can be calculated by McCumber theory.[28] The formula is:

$$\sigma_{em}(\lambda) = \sigma_{abs}(\lambda)\left(\frac{Z_l}{Z_u}\right)\exp\left(\frac{E_{ZL} - hc\lambda^{-1}}{k_B T}\right)$$

where E_{ZL} is the energy gap between the lowest Stark level of the ground-state manifold and the lowest Stark level of the upper manifold, k_B is the Boltzmann constant, T is temperature (T = 298 K), and Z_l and Z_u are the partition functions of the lower and upper manifolds, respectively. E_{ZL} is the energy corresponding to the peak wavelength of the absorption, and can be obtained from the following equation:

$$E_{ZL} = \frac{hc}{\lambda_{peak\text{-}abs}}$$

The coordination of Ho^{3+} in a variety of hosts is nearly the same, so Z_l/Z_u can be taken as 0.91, as reported in ref. 29. Fig. 9 shows the absorption and emission cross-sections of the Ho^{3+}:$^5I_7 \rightarrow {}^5I_8$ transition. The maximum absorption cross-section of Ho^{3+} at 1944 nm is 5.76 × 10^{-21} cm^2, and the maximum emission cross-section at 2030 nm is 7.13 × 10^{-21} cm^2. The emission cross-section is larger than that of fluoride glass and germanate glass, indicating that the gain medium is more conducive to laser output at around 2.0 μm.

$\sigma_{em} \times \tau_{rad}$ is an important indicator for measuring the performance of the gain medium. The larger the value, the better the performance of the gain matrix material. Table 5 presents a comparison of $\sigma_{em} \times \tau_{rad}$ of this sample with other glass systems doped with Ho^{3+} ions. The value of $\sigma_{em} \times \tau_{rad}$ in this glass system is 38.36 × 10^{-21} cm^2 ms, which is larger than that of other glasses, indicating that this glass system has excellent gain performance.

The gain coefficient is also one of the important indicators for evaluating the gain performance of a laser gain medium. The gain coefficient of the laser medium can be deduced using the following formula:[31]

$$G(\lambda) = N \times [P \times \sigma_{em} - (1 - P) \times \sigma_{abs}]$$

where P is the population inversion parameter fractional factor of the excited Ho^{3+} at the $^5I_7$ level, and N is the concentration of doped rare-earth ions, which can be calculated using the following equation:

$$N = \frac{\rho M(\mathrm{Re}^{3+})}{M} \times N_A$$

where ρ, M, $M(Re^{3+})$ and N_A, respectively, represent the sample density, the sum of the average molecular weights of the components in the sample, the molar percentage concentration

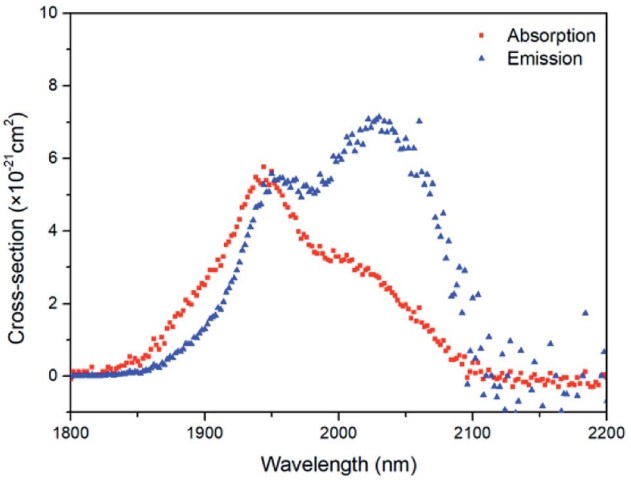

Fig. 9 Absorption and emission cross-sections of Tm^{3+}/Ho^{3+} co-doped glass.

Table 5 The σ_{em}, τ_{rad} and $\sigma_{em} \times \tau_{rad}$ of Ho^{3+} ion doping in different glass substrates

Glass host	σ_{em} ($\times 10^{-21}$ cm^2)	τ_{rad} (ms)	$\sigma_{em} \times \tau_{rad}$ ($\times 10^{-21}$ cm^2 ms)
Germanate glass[23]	4.0	0.36	1.44
Silicate glass[22]	7.0	0.32	2.24
Oxyfluoride[22]	5.2	—	—
PbO–Bi_2O_3–Ga_2O_3 (ref. 30)	5.44	4.79	26.06
TBBTH1.0[this work]	7.13	5.38	38.36

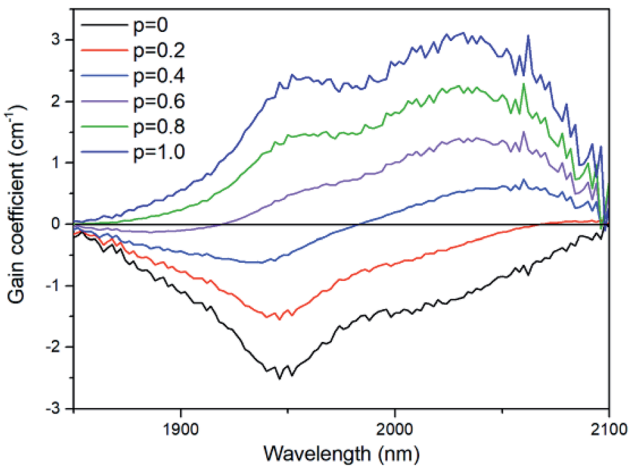

Fig. 10 Gain spectra of TBBTH1.0.

of rare-earth ions and Avogadro's constant. The gain coefficient of the TBBTH1.0 glass that we calculated is shown in Fig. 10. The maximum gain coefficient of Ho^{3+} ions in the glass sample is 3.1 cm^{-1}, which is larger than that of germanate glass (0.47 cm^{-1}), lanthanum–tungsten–tellurite glass (1.2 cm^{-1}) and fluorophosphate glass (0.66 cm^{-1}).[32–34] When the number of inverted ions increases to $P = 0.3$, the gain coefficient at 2000–2100 nm is already positive, indicating that the glass has excellent laser gain performance and a lower pumping threshold.

Conclusions

The TBB3 (67%TeO_2–17%B_2O_3–16%BaO) glass substrate, which has less phonon energy, a lower relative hydroxyl content, better thermal stability and good anti-crystallization properties, was selected as the matrix material by analyzing the Raman spectrum, infrared transmission spectrum and DTA curve.

A series of Tm^{3+}/Ho^{3+} co-doped TeO_2–B_2O_3–BaO glasses with different doping concentrations were prepared by the traditional melt-quenching technique. Through the analysis of the absorption spectra, the J–O parameters were calculated. The spontaneous radiative probability of Ho^{3+}:$^5I_7 \rightarrow {}^5I_8$ was as high as 185.85 s^{-1}. Under the pumping of an 808 nm laser diode, the optimum doping concentration for an emission peak at around 2.0 μm is Tm_2O_3: 1.0 mol% and Ho_2O_3: 1.0 mol%. For the TBBTH1.0 glass, the absorption cross-section at 1944 nm and the emission cross-section at 2030 nm of the Ho^{3+}:$^5I_7 \rightarrow {}^5I_8$ transition reach 5.76 $\times$ 10^{-21} cm^2 and 7.13 $\times$ 10^{-21} cm^2, respectively. Furthermore, the value of $\sigma_{em} \times \tau_{rad}$ of Ho^{3+} in TeO_2–B_2O_3–BaO glass is also up to 38.36 $\times$ 10^{-21} cm^2 ms. In addition, TBBTH1.0 has a lower pumping threshold and the gain coefficient of Ho^{3+} in it reaches 3.1 cm^{-1}. All of these results indicate that the prepared Tm^{3+}/Ho^{3+} co-doped TeO_2–B_2O_3–BaO glass is an ideal mid-infrared laser gain medium.

Conflicts of interest

The authors declare no conflicts of interest.

Acknowledgements

This work was supported by the National Natural Science Foundation of China (Grant No. 51772171).

References

1 G. J. Koch, M. Petros, J. Yu and U. N. Singh, *Appl. Opt.*, 2002, **41**, 1718–1721.
2 K. Scholle, E. Heumann and G. Huber, *Laser Phys. Lett.*, 2004, **1**, 285–290.
3 S. D. Jackson, F. Bugge and G. Erbert, *Opt. Lett.*, 2007, **32**, 2873–2875.
4 S. D. Jackson, *Laser Photonics Rev.*, 2009, **3**, 466–482.
5 R. Xu, J. Pan, L. Hu and J. Zhang, *J. Appl. Phys.*, 2010, **108**, 043522.
6 G. Gao, L. Hu, H. Fan, G. Wang, K. Li, S. Feng, S. Fan, H. Chen, J. Pan and J. Zhang, *Opt. Mater.*, 2009, **32**, 402–405.
7 M. Wang, L. Yi, G. Wang, L. Hu and J. Zhang, *Solid State Commun.*, 2009, **149**, 1216–1220.
8 B. Zhou, E. Y. B. Pun, H. Lin, D. Yang and L. Huang, *J. Appl. Phys.*, 2009, **106**, 103–105.
9 L. D. D. Vila, L. Gomes, C. R. Eyzaguirre, E. Rodriguez, C. L. Cesar and L. C. Barbosa, *Opt. Mater.*, 2005, **27**, 1333–1339.
10 W. Dong, Q. Yao, J. Zhang, L. Liu, J. Li and J. Wang, *Cryst. Growth Des.*, 2018, **18**, 5919–5926.
11 J. C. Sabadel, P. Armand, D. Cachau-Herreillat, P. Baldeck, O. Doclot, A. Ibanez and E. Philippot, *J. Solid State Chem.*, 1997, **132**, 411–419.
12 J. C. Sabadel, P. Armand, P. E. Lippens, D. Cachau-Herreillat and E. Philippot, *J. Non-Cryst. Solids*, 1999, **244**, 143–150.
13 N. Manikandan, A. Ryasnyanskiy and J. Toulouse, *J. Non-Cryst. Solids*, 2012, **358**, 947–951.
14 V. Nazabal, S. Todoroki, A. Nukui, T. Matsumoto, S. Suehara, T. Hondo, T. Araki, S. Inoue, C. Rivero and T. Cardinal, *J. Non-Cryst. Solids*, 2003, **325**, 85–102.
15 S. Q. Man, E. Y. B. Pun and P. S. Chung, *Opt. Commun.*, 1999, **168**, 369–373.
16 J. Lucas, *Curr. Opin. Solid State Mater. Sci.*, 1999, **4**, 181–187.
17 B. R. Judd, *Phys. Rev.*, 1962, **127**, 750–761.
18 G. S. Ofelt, *J. Chem. Phys.*, 1962, **37**, 511–520.

19 F. Huang, X. Li, X. Liu, J. Zhang, L. Hu and D. Chen, *Opt. Mater.*, 2014, **36**, 921–925.
20 H. Chen, F. Chen, T. Wei, Q. Liu, R. Shen and Y. Tian, *Opt. Commun.*, 2014, **321**, 183–188.
21 X. Liu, M. Li, X. Wang, F. Huang, Y. Ma, J. Zhang, L. Hu and D. Chen, *J. Lumin.*, 2014, **150**, 40–45.
22 K. Kadono, M. Shojiya, M. Takahashi, H. Higuchi and Y. Kawamoto, *J. Non-Cryst. Solids*, 1999, **259**, 39–44.
23 Q. Zhang, J. Ding, Y. Shen, G. Zhang, G. Lin, J. Qiu and D. Chen, *J. Opt. Soc. Am. B*, 2010, **27**, 975–980.
24 X. Fan, P. Kuan, K. Li, L. Zhang, D. Li and L. Hu, *Opt. Mater. Express*, 2015, **5**, 1356–1365.
25 Y. Tian, X. Jing and S. Xu, *Spectrochim. Acta, Part A*, 2013, **115**, 33–38.
26 M. Li, Y. Guo, G. Bai, Y. Tian, L. Hu and J. Zhang, *J. Quant. Spectrosc. Radiat. Transfer*, 2013, **127**, 70–77.
27 J. Heo, Y. B. Shin and J. N. Jang, *Appl. Opt.*, 1995, **34**, 4284–4289.
28 D. E. McCumber, *Phys. Rev.*, 1964, **134**, A299.
29 B. Zhou, E. Y. Pun, H. Lin, D. Yang and L. Huang, *J. Appl. Phys.*, 2009, **106**, 103105.
30 Y. B. Shin, J. N. Jang and J. Heo, *Opt. Quantum Electron.*, 1995, **27**, 379–386.
31 V. K. Tikhomirov, J. Méndez-Ramos, V. D. Rodríguez, D. Furniss and A. B. Seddon, *J. Alloys Compd.*, 2007, **436**, 216–220.
32 J. Fan, Y. Fan, Y. Yang, D. Chen, L. Calveza, X. Zhang and L. Zhang, *J. Non-Cryst. Solids*, 2011, **357**, 2431–2434.
33 K. Li, Q. Zhang, S. Fan, L. Zhang, J. Zhang and L. Hu, *Opt. Mater.*, 2010, **33**, 31–35.
34 Y. Tian, L. Zhang, S. Feng, R. Xu, L. Hu and J. Zhang, *Opt. Mater.*, 2010, **32**, 1508–1513.